https://doi.org/10.22226/2410-3535-2022-4-480-485

Study of the Pt-rich nanostructured FePt and CoPt alloys: oddities of phase composition

N. S. Zakharov[1], I. N. Tikchonova[1], Yu. A. Zakharov[†,1], A. N. Popova[1],
V. M. Pugachev[2], D. M. Russakov[2]

[†]ZakharovYA@iccms.sbras.ru

[1]Federal Research Center of Coal and Coal Chemistry SB RAS, Kemerovo, 650000, Russia
[2]Kemerovo State University, Kemerovo, 650000, Russia

Nanoparticles of the FePt and CoPt alloys are studied. Detailed structural-phase data on the platinum-rich nanosystems has been obtained using a combination of X-ray diffraction (XRD), selected-area electron diffraction (SAED), high-resolution transmission electron microscopy (HR-TEM) in a scanning transmission electron microscope, in addition with derivatography in coupled with the simultaneous mass spectrometry, and elemental analysis of the samples. The upper limits of Fe and Co solubility in Pt and their temperature dependencies have been defined. It is shown that, if Fe or Co contents are above the solubility limits, there is not only the diffraction-detectable phases of FCC solid solutions but also undetectable phases by XRD-method, probably, it is the intermetallic compound of $L1_2$ structure ($Fe_{1-x}Pt_{3+x}$ or $Co_{1-x}Pt_{3+x}$) or solid solution containing more amount of Fe and Co. A model of low-temperature transformation [A1-type (FCC Fe_aPt_{1-a}) → → A1 (FCC $Fe_{a-x}Pt_{1-a+x}$) + $A1_{\text{undetectable phase}}$ ($Fe_{a+x}Pt_{1-a-x}$)] when samples are heated (100 – 500°C) is proposed. The model is based on that the crystals are nano-sized and the diffusion of Fe and Co in comparison with Pt is predominant. Therefore, diffraction-undetectable phases can be existed. According to the results of derivatography and mass spectrometry methods, there is no partial oxidation of Fe and Co in the FCC phase. Therefore, oxidation is not the cause of the observed effects.

Keywords: phase composition, phase transformation, nanoparticles, nanopowders, FePt, CoPt.

1. Introduction

It is known that the phase diagrams of the FePt and CoPt systems in the nanostructured (NS) state are complicated because of a peculiar nature of the phase compositions and their transformations when alloys are heated [1 – 3]. The unique (theoretically predicted and calculated) magnetic and magneto-optical characteristics of intermetallic compounds (IC) of equiatomic compositions with a highly ordered structure $L1_0$ trigger keen and stable interest in the study of nano-sized and nano-structured FePt and CoPt alloys [4 – 5]. Despite a significant amount of published works, in fact, the problem of really achieving the predicted characteristics has yet not been solved [4 –15]. It should be noted that bimetallic systems of compositions rich in platinum are still poorly understood. Though, it has been shown that the features of phase structure, phase compositions, and their phase transformations are essential for understanding the processes of formation of relevant ICs with the $L1_0$ structure [1 – 3, 5]. In this work, for the first time, we study both the phase structure, phase compositions, and their transformations with increasing temperature, moreover nontrivial features of phase transformations are revealed.

2. Materials and experimental methods

2.1. Synthesis of the samples

Nanoparticles (NPs) of FePt and CoPt are synthesized by the co-reduction of metals from mixtures of aqueous solutions (0.1 mol/L) of $H_2PtCl_6\ 6H_2O$, $FeSO_4\ 7H_2O$, $CoCl_2\ 6H_2O$ by hydrazine (as hydrazine hydrate form) (reagents and chemicals are analytical grades). A solution of hydrazine hydrate and NaOH (pH = 13 – 14, duration of the reduction process 10 – 15 minutes, at 80°C) is added to the mixture of precursor solutions after its deaeration by argon gas sparging (argon is of special purity grade) with vigorous stirring. Obtained nanoparticles (NP) are repeatedly washed with distilled water, followed by drying in air at room temperature. NP samples have been stored in sealed glass containers.

2.2. Testing methods

The crystal and phase structure, and phase compositions of the NP have been studied by X-ray diffractometry on powder specimens prepared from samples using a Bruker D8 ADVANCE A25 high resolution diffractometer (Bruker, Germany). It is used CuK_α radiation (λ = 1.5406 Å) with

Ni-filter on a secondary (diffracted) beam. The measurements are carried out in the 2θ angular range between 20° and 140°, with a scanning step of 0.02°; at desired temperatures — in high vacuum (10^{-7} mbar) *in-situ* using high-temperature chamber HTK 1200N (temperature stability ±0.1°C) (Anton Paar GmbH, Austria). Data collection and X-ray image processing are performed using the Diffrac.Suite.Eva (V3.1) software.

X-ray phase analysis are performed using the ICDD PDF-2 database. We estimate the phase compositions according to the established earlier empirical dependences of the system composition (in the specific case of platinum content) on the average specific volume per 1 atom in the unit cell (Vat, Å³) [16]:

$$X_{Pt} = 0.033999 V_{at}^2 - 0.6068 V_{at} + 2.411 \text{ — for FePt nanoparticles} \quad (1)$$

$$X_{Pt} = 0.01378 V_{at}^2 - 0.1138 V_{at} + 0.428 \text{ — for CoPt nanoparticles} \quad (2)$$

The lattice parameters (LP) and crystallite sizes, that is the coherent scattering regions (CSRs), are calculated by the Scherrer equation using the approaches discussed in [17].

Derivatography in coupled with the simultaneous mass spectrometry has been performed on a NETSCH STA 409 PC/PG (NETSCH, Germany) in an argon atmosphere at a heating rate of 10°/min; sample weight is 10 mg.

Elemental analysis of the samples has been defined by optical emission spectrometry with inductively coupled plasma (ICP OES) using an iCAP 6500 DUO spectrometer (Thermo Scientific, USA), the radial mode of plasma observation with a power of 1150 W. The contents of the main components and impurities are determined at their characteristic wavelengths in the ranges free from spectral and other interferences. The obtained values of the concentrations of elements determined in different analytical wavelengths are averaged. In the work, the compositions of the samples, except for the selected cases, are signed in mole fractions or mole percent.

We have compared, for more preciously, the results of ICP OES with the data obtained by X-ray fluorescence analysis performed on an attachment to a Difrey 401 powder X-ray diffractometer (Burevestnik, Russia).

The electron microscopic investigation of the samples has been carried out on a JEOL JEM 2100 microscope (JEOL Ltd, Japan) in bright field mode. The details of sample preparation of highly magnetic FePt and CoPt NPs are described in [18 – 20].

3. Results and discussion

According to chemical analysis, the determined compositions for the studied samples, richest in platinum, are almost identical to assumed composition. Ni, Cu, Zn, and Si are found as impurities, the total content of which does not exceed 0.1– 0.2%.

The results of not only chemical (elemental) analysis of synthesized nanoparticles but also phase compositions of the FCC phase calculated from the XRD data are shown in the Table 1.

Typical X-ray diffraction patterns are in Fig. 1. One can see there is the only FCC phase (type A1) on the XRD patterns for all studied samples. Using expressions (1) and (2), the compositions of the FCC phases are calculated from defined LPs estimated from the XRD data.

According to the obtained results, the detected phases are platinum-rich solid solutions (SS) that are complied with the phase diagrams of the FePt and CoPt alloys. It has been established that the upper limit of the solubility of Fe and Co in platinum is 11.4 ± 0.7% and 20 ±1%, respectively (Fig. 2).

Typical SAED and HR-TEM microphotographs of FePt and CoPt samples are shown in Fig. 3. There are parallel

Table 1. Chemical composition of synthesized nanoparticles and phase compositions of the FCC phase.

Sample	FePt					CoPt				
As synthesis, mol.% according to OES ICP	Fe_7Pt_{93}	$Fe_{13}Pt_{87}$	$Fe_{15}Pt_{85}$	$Fe_{22}Pt_{78}$	$Fe_{28}Pt_{72}$	Co_6Pt_{94}	$Co_{11}Pt_{89}$	$Co_{14}Pt_{86}$	$Co_{21}Pt_{79}$	$Co_{31}Pt_{69}$
FCC, mol. % according to XRD	Fe_8Pt_{92}	$Fe_{10}Pt_{90}$	Fe_9Pt_{91}	$Fe_{12}Pt_{88}$	$Fe_{12}Pt_{88}$	Co_6Pt_{94}	Co_9Pt_{91}	$Co_{10}Pt_{90}$	$Co_{14}Pt_{86}$	$Co_{18}Pt_{82}$

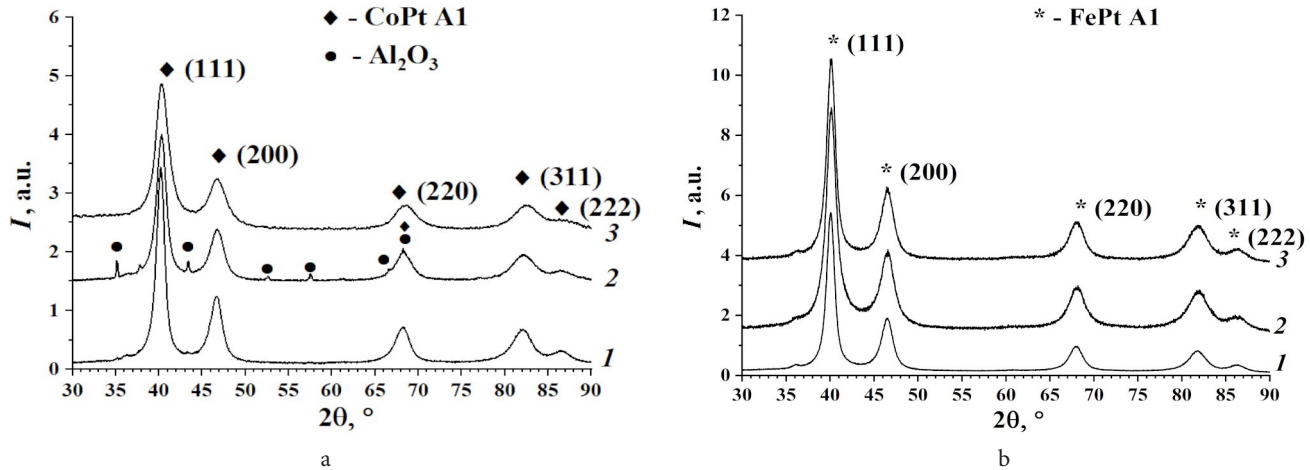

a b

Fig. 1. XRD patterns of CoPt (1 — Co_6Pt_{94}; 2 — $Co_{14}Pt_{86}$; 3 — $Co_{31}Pt_{69}$) (a) and FePt (1 — Fe_7Pt_{93}; 2 — $Fe_{13}Pt_{87}$; 3– $Fe_{28}Pt_{72}$) (b).

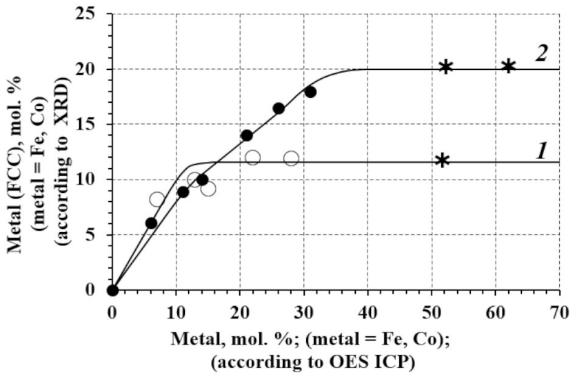

Fig. 2. Correlations between Fe (1) and Co (2) of FCC solid solution (according to XRD) and general content of Fe and Co (according ICP OES). ✱ — samples are out of this research and shown to refine upper boundaries of FCC solid solutions.

bands in all samples micro-photos, which can be naturally attributed to lattice fringes on the dominant crystal planes. For $Fe_{13}Pt_{87}$ and $Fe_{28}Pt_{72}$ samples, there are distances of 2.45 – 2.50 Å observed between lattice fringes predominantly, and for $Co_{19}Pt_{81}$, $Co_{24}Pt_{76}$ — 2.40 – 2.49 Å. It was noted that the lower boundaries of these ranges practically comply with the distances in the [110] direction for the (111) plane of the FCC lattice; the last one were calculated from the LP values determined from the XRD data (2.39 – 2.40 Å and 2.37 – 2.39 Å for FePt and CoPt, respectively). It can be concluded that the (111) crystalline faces are predominantly developed in the obtained SS. FCC structure of the synthesized NPs is also confirmed by SAED data (Fig. 3 c – f).

Considering that the upper limit of the solubility of Fe, Co in Pt is much lower than the content of Fe, Co, determined by elemental analysis, it can be assumed that while synthesis, not the only SS phase detectable by XRD, but also phases undetectable by XRD are formed. The problem of identifying this additional phase may be related to the broadening of the diffraction peaks owing to the ultra-small particle sizes. The existence of such phases is approved by the HR-TEM data. In Fig. 3a, e, there are fractions of spherical particles with sizes of 1 – 3 nm and shapeless formations of sub-nanoscale sizes, for which lattice fringes are not observed (according to HR-TEM, Fig. 3 b, f).

As for the phase compositions less than the Fe or Co solubility limits, the Fe/Pt and Co/Pt ratios in SS are close to those of the initial precursors. This is the base of the nontrivial assumption that, despite the relatively high rates of SS formation and nonequilibrium reduction processes, the compositions of NPs are close to or are in equilibrium. Consequently, the observed solubility limits (C_{lim}) are determined thermodynamically and are not related to the features of sample synthesis.

The same conclusion is made from the results of experiments on revealing the dependences of the solubility limit on temperature (for compositions with a content of $C_{(Fe, Co)} < C_{lim}$).

All the studied samples were heated stepwise with a long exposure at a given temperature. To determine the lattice parameters with the maximum possible accuracy, we approximated the peak in shape by Pearson type VII distributions. During the approximation, the doublets $K_{\alpha 1}$, $K_{\alpha 2}$ were taken into account, the values of the lattice parameters were averaged. Such approach made it possible to additionally take into account the correction for the deformation of samples with a change in temperature. The (311) peak and its temperature transformations is shown as an example, which is more responsive, in Fig. 4. The compositions of the FCC phases were calculated by (1) and (2) relations, taking into account the determined values of the thermal expansion coefficients. As a result, LPs have been determined and changes in the compositions have been detected. The established temperature-time dependences of LPs and compositions are shown in Fig. 5.

According to studies of nanoparticles when NPs are heated, it is found that with a rapid successive increase in temperature to 130, 210, and 390°C, LP values are achieved slightly variables meanings, which then, when thermostated

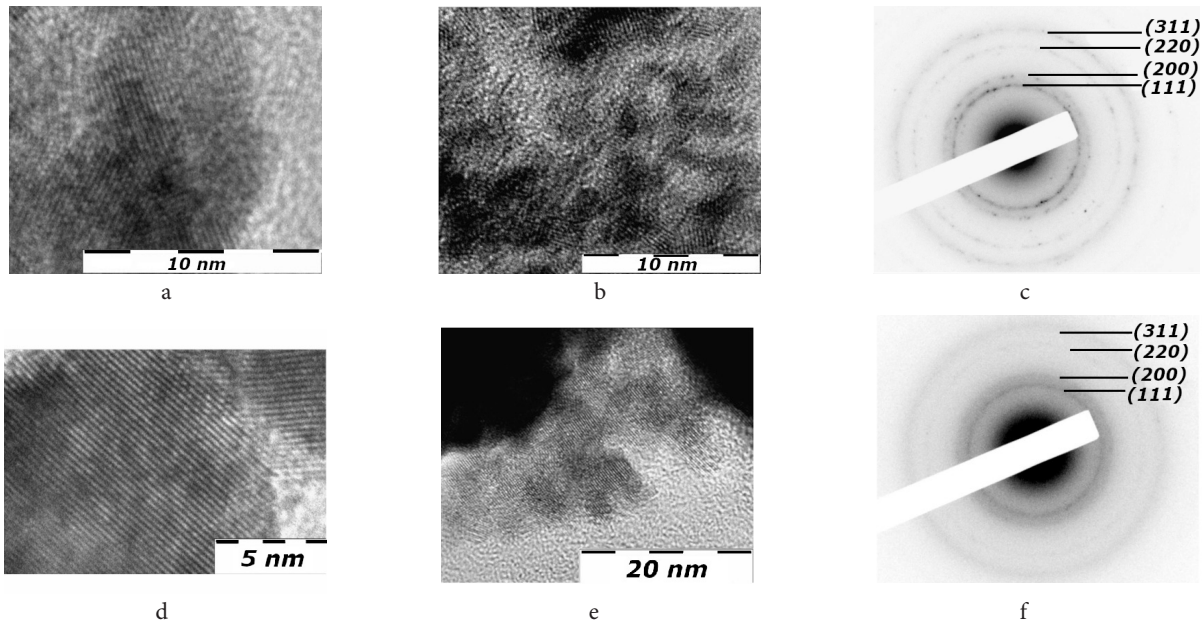

Fig. 3. HR-TEM photos of $Fe_{15}Pt_{85}$ (a, b) and $Co_{26}Pt_{74}$ (d, f); SAED patterns of $Fe_{15}Pt_{85}$ (c) and $Co_{14}Pt_{86}$ (f).

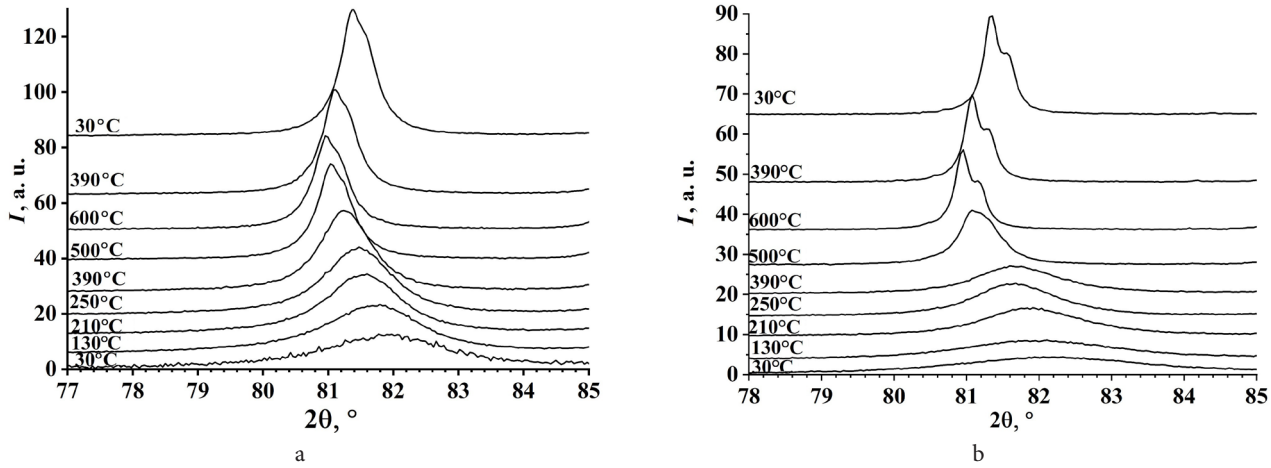

Fig. 4. Temperature transformations of (311) peak of $Fe_{15}Pt_{85}$ (a) and $Co_{14}Pt_{86}$ (b).

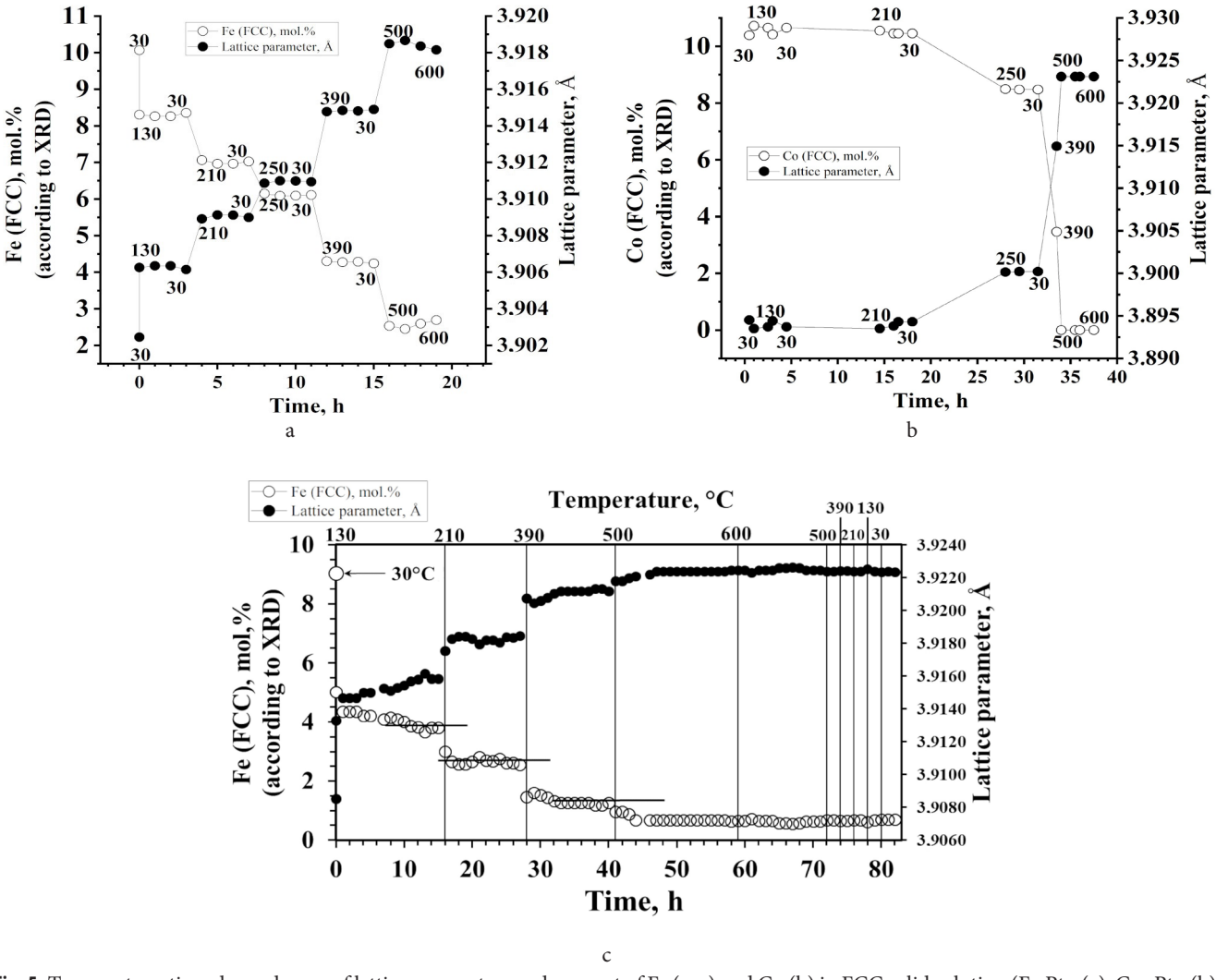

Fig. 5. Temperature-time dependences of lattice parameters and amount of Fe (a, c) and Co (b) in FCC solid solution (Fe_5Pt_{95} (a), $Co_{14}Pt_{86}$ (b) and $Fe_{15}Pt_{85}$ (c)) (a, b — temperature is above markers).

for 1 hour, slightly increase to constant values. At higher temperatures, the process of increasing the values of LPs during thermostating is not observed, thus, the compositions of the samples during thermostating are constant.

There are the dependences of LPs and compositions on temperature for all considered samples in the range $C_{Fe,Co} < C_{lim}$ in Fig. 6. These dependences are combined with fragments of phase diagrams of alloys rich in platinum [2,21,22]. According to the concepts being developed, the curves we plotted are the temperature dependences of the upper (concentration) regions of the existence of SS in NS FePt and CoPt.

On the one hand, the proximity of the system to the equilibrium state is evidenced by the constancy of the SS

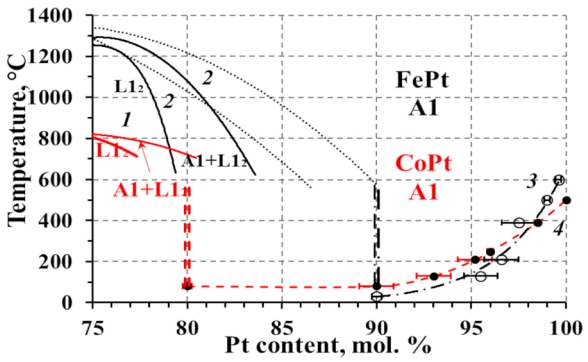

Fig. 6. (Color online) Combined phase diagrams parts of CoPt (1) and FePt (2), rich in platinum: solid curves are according to experimental data, dot curves are according to calculated values. Range of data shows upper limits of FCC solid solution of FePt (3) and CoPt (4) with approximate boundaries of CoPt (= = =) and FePt (=·=·=).

compositions while long-term thermostating (Fig. 5). On the other hand, this is supported by the established practical independence of the upper limit of solubility on the initial composition of the samples (Fig. 6). For systems richer in platinum, Fe_5Pt_{95}, Fe_7Pt_{93}, Co_6Pt_{94}, when heated to 130°C (Fig. 6), there are no changes in LP, and, as a consequence, SS compositions are constant. But when the figurative point is in the temperature range outside the temperature boundaries of monophasic state (Fig. 6), the LP values change with an increase in the heating temperature according to the temperature-time dependences shown in Fig. 5.

Thus, a natural model of the processes that occur when systems are heated and lead to the described above results is the transformation of systems from a single-phase state of A1-structure into a two-phase state. As A1 phases of high Fe and Co amount are undetectable by XRD, we approximate their temperature dependencies, as shown in Fig. 6. The assumed ideas about the practical equilibrium of the obtained nanosystems are nontrivial, since the systems under study are synthesized in the nanoscale state, and the transition from one phase state to another occurs at low temperatures at high rates. The implementation of both cases is possible only for NPs of FCC solid solutions: according to the results of HR TEM and measurements of CSRs values, their sizes are approx. 4–10 nm. Their transformation into a two-phase state can be carried out only by diffusion of the components with the formation of diffraction-undetectable nanophases.

It is known that the values of the diffusion coefficients of Fe, Co and Pt in different media differ significantly, but the ratio $D(\mathrm{Fe}) \approx D(\mathrm{Co}) \gg D(\mathrm{Pt})$ is always preserved. Obviously that distances of several nm in length corresponding to the diffusion length to the periphery of the SS region. Thus, it takes approx. 1–2 hours Fe and Co to "overcome" this distance. This time is comparable with the times for reaching constant values of composition limits in Fig. 5 [23,24]. The nature of the temperature dependence of the upper boundaries of the FCC SS shows that the model of phase transformations is realized owing to the diffusion of Fe or Co from the SS region.

Therefore, the proposed model of phase transformations at low temperatures can be implemented only in nanosized objects, and as has demonstrated, its implementation under these conditions is likely. We propose this model for the first time. Though, there are questions that require additional studies to specify the boundaries of the phase compositions of Fe Pt [2] and Co Pt [21,25].

Considering the nontriviality of the obtained results, and the proposed model for their explanation, experiments have been performed to determine the possibility of the selective oxidation of Fe and Co in our conditions (high vacuum) in the NPs of the FCC solid solution. In Fig. 7, it is indicated the results of derivatography and mass spectrometry, which are typical for all samples in the range of compositions $C_{(\mathrm{Fe,Co})} < C_{\mathrm{lim}}$. It follows from them that, in the presence of trace amounts of oxygen in the carrier gas (Ar), there is no increasing in the mass of the samples as a result of almost complete oxidation (according to Fig. 5) of Fe and Co contained in the samples in the region up to 500 – 600°C. The DTA curves show the endothermic nature of the processes occurring up to 500 – 600°C, which contradicts the exothermic process of oxidation of Fe and Co, and can probably be explained by the implementation of phase transformations in NPs.

The process of oxidation (it is the well-known kinetics of the "parabolic law of oxidation") does not correspond to the actual kinetics of the transformation either (Fig. 5). On the X-ray patterns, there is no increase in the intensities of

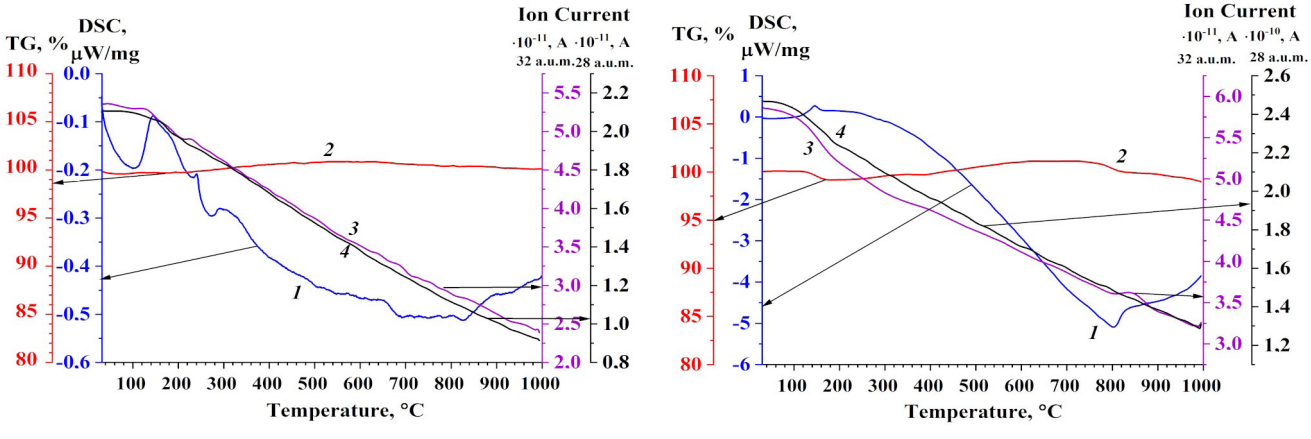

Fig. 7. (Color online) DSC (1), TG (2) curves and mass-spectra of gases evolved during heating — O_2 (32 a.u.m.) (3), N_2 (28 a.u.m.) (4) for $Fe_{13}Pt_{87}$ (a) and $Co_{26}Pt_{74}$ (b).

the phases of metal oxides during heating of the samples. In addition, according to electrochemistry, the oxidation potentials of solid solutions rich in one of the components are linearly dependent on their compositions and, accordingly, for Fe(Co)·Pt solid solutions should differ slightly from the oxidation potential of noble platinum. The foregoing is a powerful argument against the possibility of explaining the results in Fig. 5 oxidation of less noble components in SS.

4. Conclusions

The study of the structural-phase properties of nanostructured FePt and CoPt powders, rich in platinum, obtained by the method of co-reduction from mixtures of precursors solutions was performed for the first time. A number of features of the phase compositions have been established:

1. the upper limit of the solubility of Fe and Co in Pt and the composition with monophasic state have been found;
2. the occurrence of phase transformations of the type A1-type (FCC Fe_aPt_{1-a}) → A1 (FCC $Fe_{a-x}Pt_{1-a+x}$) + + $A1_{\text{undetectable phase}}$($Fe_{a+x}Pt_{1-a-x}$) has been revealed;
3. the proposed model of phase transformations occurs at relatively low temperatures (100 – 600°C) with significant rates of phase transformations.

Acknowledgements. The authors sincerely thank DL. M. Khitsova for the results of the derivatography, and R. P. Kolmykov for elemental analysis by optical emission spectroscopy. The work was performed using the equipment of the FRC CCC SB RAS within the framework of the state task (project 117041910151-9).

References

1. Z. Sun, D. Zhao, X. Wang et al. J. Alloys Compd. 870, 159384 (2021). Crossref
2. Z. Wen, Y. Wang, C. Wang. Int. J. Mater. Res. 113 (5), 428 (2022).Crossref
3. C. Jongjaihan, A. Kaewrawang. Micromachines. 13 (10), 1559 (2022). Crossref
4. D. Kaya, I. Adanur, M. Akyol, et. al. J. Mol. Struct. 1224, 128999 (2021). Crossref
5. J. E. Wittig, J. Bentley, L. F. Allard. Ultramicroscopy. 176, 218 (2017). Crossref
6. W. Pei, D. Zhao, C. Wu et al. ACS Appl. Nano Mater. 3 (2), 1098 (2020). Crossref
7. U. Bozuyuk, E. Suadiye, A. Aghakhani et al. M. Sitti. Adv. Funct. Mater. 32 (8), 2109741 (2022). Crossref
8. D. Li, N. Poudyal, V. Nadwana, et al. J. App. Phys. 99 (8), 08E911 (2006). Crossref
9. R. Medwal, N. Sehdev, S. Fyyapoorni. Appl. Phys. A. 109 (2), 403 (2012). Crossref
10. J. Li, S. Sharma, X. Liu et al. Joule. 3 (1), 124 (2019). Crossref
11. M. Islam, M. S. I. Sarker, T. Nakamura et al. Mater. Chem. Phys. 269, 124727 (2021). Crossref
12. B. Bian, G. Chen, Q. Zheng et al. Small. 14 (34), 1801184 (2018). Crossref
13. X. Zhang, F. Zhang, Y. Zhang et al. J. Supercond. Nov. Magn. 31 (8), 2553 (2018). Crossref
14. A. Lyberatos. Phys. B: Condens. Matter. 576, 411741 (2020). Crossref
15. F. M. Abel, V. Tzitzios, E. Devlin et al. ACS Appl. Nano Mater. 2 (5), 3146 (2019). Crossref
16. V. M. Pugachev, Yu. A. Zakharov, A. N. Popova et al. J. Phys. Conf. Ser. 1749 (1), 012036 (2021). Crossref
17. Yu. A. Zakharov, V. M. Pugachev, K. A. Korchuganova, et. al. J. Struct. Chem. 61 (6), 994 (2020). Crossref
18. N. S. Zakharov, A. N. Popova, Y. A. Zakharov. J. Phys. Conf. Ser. 1749 (1), 012012 (2021). Crossref
19. Yu. A. Zakharov, N. S. Zakharov, A. N. Popova, et. al. Butlerov Comm. 67 (7), 79 (2020). (in Russian) Crossref
20. N. S. Zakharov, A. N. Popova, Yu. A. Zakharov, et. al. Chem. Phys. 41 (7), 84 (2022). (in Russian) Crossref
21. T. Mehaddene, E. Kentzinger, B. Hennion et al. Phys. Rev. B. 69 (2), 024304 (2004). Crossref
22. H. Okamoto: Phase Diagrams of Binary Iron Alloys. V. 9, 1st ed. ASM International (1993) 472 p.
23. S. I. Konorev, R. Kozubski, M. Albrecht et al. Comput. Mater. Sci. 192, 110337 (2021). Crossref
24. O. Ersen, C. Goyhenex, V. Pierron-Bohnes. Phys. Rev. B. 78 (3), 035429 (2008). Crossref
25. P. Andreazza, V. Pierron-Bohnes, F. Tournus, et al. Surf. Sci. Rep. 70 (2), 188 (2015). Crossref